Journal of Geodesy (2026) 100:21
https://doi.org/10.1007/s00190-026-02046-9

ORIGINAL ARTICLE

Calibration of the GOCE accelerometers by GPS- and SLR-based precise orbit determination

P.N.A.M. Visser[1] · J.A.A. van den IJssel[1] · C. Siemes[1]

Received: 5 November 2025 / Accepted: 21 February 2026 / Published online: 11 March 2026

Abstract
The ESA GOCE satellite carried a gravity gradiometer consisting of three pairs of accelerometers on mutually orthogonal axes. For each accelerometer, bias and scale factors have been re-estimated by a dynamic precise orbit determination (POD) using improved gravity field modeling and standards. The kinematic orbit solution included in GPS-based Precise Science Orbit (PSO) product served as the baseline observables for 1210 daily arcs, covering the period from 1 November 2009 to 20 October 2013. Implementing improved force models almost completely resolved the deviations of the *Y*-axis scale factor obtained in earlier work (Visser and Ijssel 2016). A novel aspect is the verification by comparison with dynamic POD solutions based on SLR observations using 51 two-day orbital arcs. A high level of consistency was obtained between the kinematic PSO- and SLR-based accelerometer calibration parameters, e.g. within 0.01 nm/s^2 for the *X*-axis pointing predominantly in the flight direction in terms of bias. One set of accelerometer scale factors was estimated for the entire mission. These were found to be consistent to within 0.005 for all accelerometer axes. The three-dimensional consistency between the dynamic orbits and the PSO reduced-dynamic orbit solutions has a mean Root-Mean-Square (RMS) of 4.5 and 10 cm, respectively, for the PSO reduced-dynamic and SLR-based dynamic orbit solutions. In addition, the one-dimensional RMS-of-fit of the PSO kinematic orbit solution improved significantly from 6.9 in Visser and Ijssel (2016) to 2.6 cm.

Keywords GOCE · Accelerometer · Calibration · Precise orbit determination · Bias · Drift · Kinematic orbits · GPS · SLR

1 Introduction

The Gravity field and steady-state Ocean Circulation Explorer (GOCE) was the first European Space Agency (ESA) Earth Explorer satellite, launched on 11 March 2009 (Balmino et al. 1999). More than four years of successful mission operations ended on 11 November 2013, when GOCE re-entered the atmosphere. The primary payload of GOCE was the gravity gradiometer, consisting of three pairs of electrostatic accelerometers on three mutually orthogonal axes, aligned predominantly with the flight (*X*-axis), cross-track (*Y*-axis) and radial (*Z*-axis) directions, with an arm length of about 50 cm (distance between two accelerometers on the same axis), and centered around the spacecraft's center-of-mass. The gradiometer was designed to provide high-quality observations in a frequency range of 5-100 mHz. For mission success, it was essential to very precisely calibrate the scale factors of the accelerometers, for which an on-orbit shaking procedure was implemented (Cesare and Catastini 2005). The gradiometer provided the observations for deriving very precise Satellite Gravity Gradient (SGG) measurements in the above mentioned frequency range, for which there was no direct need to know the accelerometer biases. However, the gradiometer also provides observations for deriving the so-called common-mode accelerometer measurements which are needed together with the Global Positioning System (GPS) Satellite-to-Satellite Tracking (SST) observations for estimating the low-degree spherical harmonic gravity field coefficients (Pail et al. 2011). To this aim, precise values for the common-mode accelerometer biases are to be established or estimated as well, which is typically based on Precise Orbit Determination (POD) using GPS observations, either directly from SST observations or from very

✉ P.N.A.M. Visser
P.N.A.M.Visser@tudelft.nl

J.A.A. van den IJssel
J.A.A.VandenIJssel@tudelft.nl

C. Siemes
C.Siemes@tudelft.nl

[1] Faculty of Aerospace Engineering, Delft University of Technology, Kluyverweg 1, Delft 2629HS, The Netherlands

precise kinematic orbit solutions (Visser and Ijssel 2016). The common-mode accelerometer observations are obtained by taking the average of the observations of accelerometers 1 and 4 for the X-axis, 2 and 5 for the Y-axis, and 3 and 6 for the Z-axis (Fig. 1).

When producing gravity field models typically accelerometer calibration parameters are estimated together with the gravity field coefficients and often also many nuisance parameters (for example so-called empirical accelerations). In that case, the aim is to obtain the best possible gravity field solutions and not so much to obtain the best possible accelerometer calibration parameters. The accelerometer calibration parameters will then typically be less reliable because there will also be an interplay/correlation with the nuisance parameters and the primary objective is to avoid that non-gravitational signals end up in the gravity solutions. Having reliable accelerometer calibration parameters is a prerequisite for deriving thermosphere mass density and winds from the accelerometer observations (Siemes et al. 2023).

In Visser and Ijssel (2016) it was shown that precise accelerometer calibration parameters can be obtained for all individual accelerometers after applying center-of-mass offset corrections, which are necessary because of the angular motion of the GOCE satellite and because of gravity gradients. The estimated daily accelerometer biases were found to be consistent with those obtained for the common-mode accelerometer observations and also with the biases of the SGG observations. In addition, the different behavior of the individual accelerometers could be observed, with distinct differences for the sensitive and less sensitive axes. Moreover, the proper calibration of the accelerometers by the on-board shaking procedure could be confirmed for the X- and Z-axis scale factors. The scale factor for the Y-axis was found to be deviating by about 0.03, suspected to be due to remaining dynamic force model errors.

The availability of improved Precise Science Orbit kinematic solutions (Arnold et al. 2023) and improved (pseudo-)static and temporal gravity field models, such as GOCO06s and EIGEN-GRGS.RL04.MEAN-FIELD (Kvas et al. 2021; Lemoine et al. 2019) triggered a reprocessing of the POD-based accelerometer calibration. In addition, updated IERS standards were employed (Petit and Luzum 2010) and a more recent ocean tides model was used in the orbit determinations, GOT 4.10 (Ray 2013).

In addition to a GPS receiver for high-low Satellite-to-Satellite tracking, GOCE is equipped with laser retro-reflectors (LLR) for Satellite Laser Ranging (SLR). Typically, SLR observations are used for validating the GPS-based precise orbit solutions (Arnold et al. 2023). However, the SLR observations can be used for precise orbit determination as well and early work showed promising results for the Low-Earth Orbiting (LEO) CHAMP satellite, where improved results were obtained when using accelerometer observations to represent the non-gravitational accelerations (Bruinsma et al. 2003). Therefore, SLR-based dynamic POD was used for an independent verification of the GPS or PSO-based dynamic POD accelerometer calibration results. At the same time, an assessment could be made of how precisely GOCE orbits can be computed using the relatively sparse SLR tracking of this very low flying satellite.

An overview of the used data sets, including SLR observations, is presented in Sect. 2. The methodology, including the setup used when processing SLR observations, is summarized in Sect. 3. Results and conclusions are provided in Sects. 4 and 5, respectively.

2 Observations

As described in Visser and Ijssel (2016), the kinematic PSO solutions have been used as the observations for the estimation of accelerometer calibration parameters. These kinematic PSO solutions consist of time series of X, Y, and Z coordinates in an Earth-centered, Earth-fixed (ECF) reference frame and can be seen as a condensed set of the original GPS SST pseudo-range and carrier phase observations, where no use is made of force models for the LEO satellite. Use has been made of the official GOCE version *0201* release of the SST_PSO product (ESA 2025; Arnold et al. 2023), which includes kinematic orbit solutions with an interval of 1 s for the time series of coordinates. For the GOCE accelerometer observations and the attitude quaternions, use has been made of the official GOCE version SST_PSO *0202* release of the EGG_CCD and EGG_IAQ products, which provide time series with a nominal time interval of 1 s as well (ESA 2025). Please note that the merged attitude quaternion product was used, which is based on a combination of star tracker observations and rotational motion derived from the accelerometer observations. It is noted that the merged quaternion product is obtained by low-pass filtering the star tracker observations and using the differential accelerometer observations for the higher frequencies (Frommknecht et al. 2011). This means that accelerometer biases do not affect the attitude quaternion product. Moreover, it will be shown in Sect. 4.2 that the scale factors have been properly calibrated. The selected data cover the entire period of GOCE science operations from 1 November 2009 to 20 October 2013.

The six accelerometers of the gradiometer are schematically displayed in Fig. 1 (see also Visser (2009) and Visser and Ijssel (2016)). The locations of the accelerometers are indicated along the X-, Y- and Z-axes of the Gradiometer Reference Frame (GRF). For each accelerometer, the two ultra-precise axes and one less precise axis are indicated. The attitude quaternions provide the information for rotating the accelerometer observations from the GRF to the J2000 reference frame.

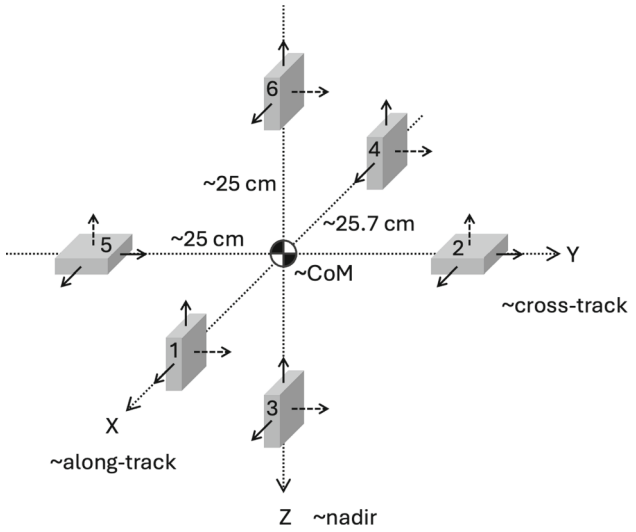

Fig. 1 Configuration and naming convention of the three orthogonal pairs of accelerometers that form the GOCE gravity gradiometer. Note the arm lengths of about 50.0 (Y- and Z-axes) or 51.4 cm (X-axis)(Cesare and Catastini 2005)). The sensitive and less sensitive axes are indicated as well (respectively, by the solid and dashed arrows)

Satellite Laser Ranging (SLR) observations in the form of normal points were taken from the International Laser Ranging Service (ILRS) Crustal Dynamics Data Information System (CDDIS) and EUROLAS Data Center (EDC) servers (Pearlman et al. 2019; Noll et al. 2019). The used GOCE SLR observations were collected by 20 stations, which are displayed in Fig. 2. The SLR data also cover the full GOCE operational mission period from 1 November 2009 to 20 October 2013, although the tracking by SLR is in general quite sparse: the number of observations per day is very variable and can range from zero to more than 200.

3 Methodology

For the PSO-based accelerometer calibration, the same methods are used as described in Visser and Ijssel (2016). Accelerometer biases and scale factors were estimated for both the common-mode and individual accelerometer observations, where the latter need to be corrected for rotational and gravity gradient terms. The associated corrections were computed in exactly the same way as in Visser and Ijssel (2016), Equations (1)-(5), with the exception that for the gravity gradient terms a more recent gravity field model was used (Table 1). The fundamental equation from Visser and Ijssel (2016) representing the accelerometer observations is included here for easy reference:

$$\mathbf{d} = \mathbf{S}_i^{-1}(\mathbf{a}_{\mathrm{obs},i} - \mathbf{b}_i - \epsilon_i) - (\Gamma + \mathbf{R})\mathbf{x_i} \quad (1)$$

where $\mathbf{d}$ represents the linear nog-gravitational accelerations, $\mathbf{S}_i$ represents the 3×3 diagonal scale factor matrix, and $\mathbf{a}_{\mathrm{obs},i}$, $\mathbf{b}_i$, ϵ_i, respectively, the three-dimensional vectors of observations, biases and observation errors, all for accelerometer i (i=1,..,6). It is noted that a diagonal structure for the scale factor matrix is used since the off-diagonal elements are expected to be very small due to the use of already calibrated accelerometer data (Siemes et al. 2019). Moreover, the requirement for the combination of misalignments and cross-coupling terms is that they are below 1.3×10^{-4} (Cesare and Catastini 2005). In fact, it is expected that the scale factors are very close to unity. The gravity gradient tensor and matrix with rotational terms are represented by Γ and $\mathbf{R}$. The offset of accelerometer i with respect to the satellite's center of mass is indicated by $\mathbf{x}_i$. It is noted that for computing this offset the precisely known values for the arm lengths have been used (included in Table 1). It is assumed that the center of the gradiometer coincides with the center-of-mass of the satellite (Floberghagen et al. 2011).

As mentioned in Sect. 1, for the reprocessing use was made of the improved (pseudo-)static and temporal gravity field models EIGEN-GRGS.RL04.MEAN-FIELD or GOCO06s (Kvas et al. 2021; Lemoine et al. 2019). The EIGEN-GRGS.RL04.MEAN-FIELD model includes trend, annual and semi-annual gravity field coefficients with different validity periods (including the period of GOCE science mission operations). For obtaining the time variable gravity field coefficients of this gravity field model, use was made of a fitting process of the GRACE monthly gravity field solutions. The GOCO06s model also includes temporal gravity field terms, but only one set of trend and annual gravity field coefficients. In addition, the GOT 4.10 model was used to represent the perturbing GOCE accelerations caused by ocean tides (Ray 2013). The GRACE de-aliasing product release 6 from the Helmholtz GeoForschungsZentrum (GFZ) was selected to represent further additional field changes caused by the oceans and atmosphere (GRACE 2018; Dobslaw et al. 2017). It is noted that the accelerometer measurements in principle capture the non-gravitational accelerations that are left by the Drag-Free Control (DFC) resulting in very small remaining accelerations along especially the X-axis (*c.f* Figure 2 in (Visser and Ijssel 2016)). The most recent publicly available GEODYN version 1911 (Nicholas et al. 2025; NASA 2025) was used for the POD (Pavlis et al. 2015), allowing the adoption of updated IERS standards, e.g., for polar motion (Petit and Luzum 2010). An overview of the adopted standards and dynamic models is included in Table 1.

GOCE was also equipped with laser retro-reflectors allowing SLR. Typically, SLR observations are used for quality checking the orbit solutions based on the GPS SST tracking observations. The consistency with the SLR observations is at a level of about 1.8 and 2.4 cm for the reduced-dynamic and kinematic PSO solutions (Arnold et al. 2023). As men-

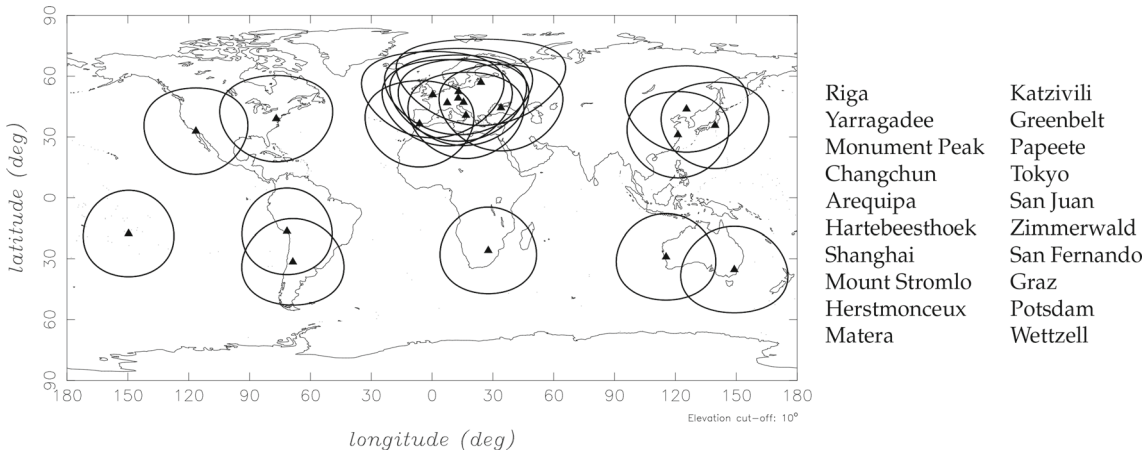

Fig. 2 Global network of SLR stations selected for GOCE. The visibility circles are indicated for an elevation cutoff angle of 10°. The names of the selected stations are included on the right

tioned above, the SLR tracking is quite sparse for GOCE. However, only a few parameters need to be estimated in the POD-based accelerometer calibration. For GOCE, typically only the initial state (begin position and velocity) and accelerometer biases per axes are estimated, i.e. nine parameters in total (Visser and Ijssel 2016) per orbital arc. It has been shown that accelerometer scale factors can be estimated as well for longer periods if such periods include orbit maneuvers, which would mean three additional parameters. Given the small number of estimated parameters, it is interesting to explore the possibility for estimating accelerometer calibration parameters by SLR-based POD. This allows a verification of the GPS- or kinematic PSO-based estimation. The concept of SLR-based POD using accelerometer observations for representing the non-gravitational accelerations was already tested a few decades ago for CHAMP (Bruinsma et al. 2003). The state-of-the-art at that time resulted in a Root-Mean-Square (RMS) of fit of around 17 cm for the SLR observations and a three-dimensional RMS of orbit differences of around 8 m with GPS-based orbit solutions. For CHAMP, use was made of orbital arcs with a duration of 2 days for which the average number of SLR observations was about 375. For GOCE, use was made of two-day arcs as well in order to have a sufficient number SLR tracking observations for the parameter estimation (see also Sect. 4).

SLR station coordinates were derived from ITRF2020 (Altamimi et al. 2023), with station displacements caused by ocean loading based on the FES 2014 ocean tides model (Lyard et al. 2021) using the Chalmers loading calculator (Chalmers 2025). Furthermore, tropospheric corrections, the SLR center-off-mass offset in the Satellite body Fixed Frame (SRF) and a geometric LLR correction were taken into account (Table 1). It is noted that the GOCE center-of-mass changes due to fuel consumption were taken into account for deriving the SLR center-of-mass offset. Table1 includes the associated values at the start (BOL) and end of the mission (EOL).

4 Results

The several updates mentioned in Sect. 3 were implemented and used for estimating a new set of GOCE calibration parameters for both the common-mode and individual accelerometers. As outlined above, an extra set of accelerometer calibration parameters was derived using SLR observations. In the baseline approach, only biases are estimated for the accelerometers (Sect. 4.1). In addition, accelerometer scale factors have been estimated as well for the entire period of GOCE science operations (Sect. 4.2). The results discussed in this section have nominally been obtained using the EIGEN-GRGS.RL04.MEAN-FIELD gravity field model complete to degree and order 200.

4.1 Accelerometer biases

First, accelerometer biases were estimated using the kinematic PSO solutions. In total, 1210 daily arcs were identified without gaps in the GPS, accelerometer and star tracker data larger than 15 min, compared to 1213 daily arcs in Visser and Ijssel (2016). Three more days were deselected because of gaps in the reprocessed kinematic PSO solutions. It is noted that a uniform weighting scheme was adopted, where all kinematic coordinates are weighted equally. A 5σ data editing was applied in the POD, which means that kinematic coordinates were eliminated for which the absolute observation residuals are larger than 5 times the RMS-of-fit. On the average, this resulted in eliminating 0.2% of the kinematic coordinates with a minimum of 0% and a maximum of 3.6%

Table 1 Standards and models used for the GOCE orbit and SLR data reduction and estimation of accelerometer bias parameters

Reference System	
Polar motion and UT1	IERS EOP 05 C04 (IAU2000A) series with IERS 2010 daily and sub-daily corrections
Precession & Nutation model	IERS Conventions 2010 (Petit and Luzum 2010)
Dynamic models	
Gravity field	EIGEN-GRGS.RL04.MEAN-FIELD or GOCO06s complete to degree and order 200 including time variable gravity field terms (Kvas et al. 2021; Lemoine et al. 2019)
Solid Earth tides	IERS Conventions 2010 (Petit and Luzum 2010)
Pole tide	IERS Conventions 2010 (Petit and Luzum 2010)
Ocean tides	GOT 4.10, update to Ray (1999, 2013)
Third bodies	Sun, Moon, Venus, Mars and Jupiter (DE-405) (Standish 1998)
Atmosphere and ocean	GRACE de-aliasing product release 6 from GFZ (GRACE 2018; Dobslaw et al. 2017)
Gradiometer	
Arm length	514.01350/499.89000/500.20100 (X/Y/Z/ mm)
SLR	
Observations	Normal points from EUROLAS Data Center (EDC) and NASA Crustal Dynamics Data Information System (CDDIS) (Noll et al. 2019)
Station coordinates	SLRF2020 derived from ITRF2020 (Altamimi et al. 2023)
Ocean loading	SLR station coordinates are corrected for ocean loading using the Chalmers loading calculator (Chalmers 2025) with the FES2014 tide model (Lyard et al. 2021)
Laser Retro-Reflector	Offset with respect to center-of-mass (SRF)
(LRR)	BOL 17/03/2009 (X/Y/Z mm): 2407.6/−3.6/558.0
	EOL 11/11/2013 (X/Y/Z mm): 2370.6/−3.6/558.0
SLR geometric correction	Offset LRR optical center with respect to LRR reference point along the Z-axis of the satellite body fixed frame: −1.9 cm
Troposphere correction	According to (Mendes et al. 2002)
Elevation angle cutoff	10°

toward the end of the GOCE science mode operations when solar activity was high (see also below).

The resulting time series of the biases are displayed in Figs. 3 and 4. These Figures include estimates of a bias at the epoch of 1 November 2009 and a bias drift for each axis obtained by a linear regression of the daily values. Note that these Figures also implicitly show how the selected days cover the GOCE period of science mode operations, including a gap in the summer of 2010 due to an onboard anomaly. Both values for the individual accelerometers and for the common-mode accelerations are shown. It can be observed that the values for the individual accelerometers and the common-mode accelerations are consistent to a high level. This is corroborated by the values included in Table 2. The average of the values in this table in *italics* should ideally be equal to the ones derived for the common-mode accelerometer observations. For the $X-$ and Y-axes (predominantly along-track and cross-track) this is indeed the case to within 0.012 nm/s^2 and 0.0001 nm/s^2/day for the bias and drift. For the Z-axis the consistency is about 1.2 nm/s^2 and 0.003 nm/s^2/day, respectively. Please note again that each accelerometer has a less sensitive axis, indicated in **boldface**, reflected also by much higher bias and drift values.

As mentioned in Sect. 3, the orbital arcs for SLR have a duration of two days. Only two-day periods were selected for which at least 75 SLR observations are available for each day. This criterion leads to 51 two-day arcs spread out over all years of GOCE science mode operations. The mean number of observations is equal to 226, with a minimum of 157 and a maximum of 339. The number of SLR stations varied between 3 and 10 with an average of about 6. The number of tracking passes varied between 7 and 18 with an average of about 12. The SLR station coordinates were kept fixed and no SLR range biases were estimated. Also for the SLR-based POD a uniform observation weighting was adopted and a 5σ data editing was applied in addition to a 10° elevation cutoff (Table 1). A total of 11728 SLR normal points are available for the selected 51 two-day arcs. The 5σ data editing resulted in the elimination of 26 observations, i.e. about 0.2%. The 10° elevation cutoff resulted in the elimination of 158 observations or about 1.3%. For SLR, only biases for the common-mode accelerometer observations were estimated. The PSO-based results show that a similar performance can be expected for the individual accelerometers in terms of estimability and POD performance.

Figure 4 and Table 2 include the bias and drift values for the SLR-based POD as well. The associated values are very close to the PSO-based values for the X-axis: to within about 0.01 nm/s^2 and 0.0002 nm/s^2/day for the bias and drift, respectively. For the Y- and Z-axes, the differences are about 17 and 50 nm/s^2 for the bias, and about 0.03 and 0.0012 nm/s^2/day for the drifts obtained by the linear regression. Although for some accelerometers, the linear model does not

capture the time series very well, especially at the start of science mission operations, the bias differences are, in general, much smaller than the RMS-of-fit values displayed in Fig. 4, except for the Y-axis for which the difference is at about the level of the RMS-of-fit. The RMS-of-fit of the linear regression for the SLR-based accelerometer biases along the Z-axis is large at a level of about 100 nm/s^2, which shows that the bias cannot be determined accurately for this direction. This is confirmed by the formal errors for the estimated biases, which are typically about a factor 1000 larger for the z-axis as compared to the formal errors for the X-axis. Also, for SLR, it can be seen how the selected 51 two-day arcs cover the GOCE period of science mode operations with relatively many arcs at the beginning and a decaying number of arcs closer to the end when GOCE was flying at a significantly lower altitude. This lower altitude made it more challenging for SLR stations to track GOCE, and possibly less priority was given to tracking GOCE by a number of SLR station operators in the course of the mission.

As mentioned above, the baseline results were obtained with the EIGEN-GRGS.RL04.MEAN-FIELD model, which includes temporal gravity field coefficients (trend, annual and semi-annual) with different validity periods, including the GOCE period of science mode operations. In addition, the GOCO06s model has been used to process the common-mode accelerometer observations. The observations used to produce the GOCO06s model include the entire GOCE data set. However, only one set of temporal gravity field coefficients was derived representing the average trend and annual gravity field changes for a period of 15 years including the GOCE operational phase. The resulting time series of the biases are included in Fig. 4. Rather pronounced yearly variations can be observed for especially the Y- and Z-axes, which are not visible when using the EIGEN-GRGS.RL04.MEAN-FIELD gravity field model. This result indicates that great care has to be taken when using temporal gravity field coefficients that are averaged over long periods of time, 15 years in this case. Larger variability of GRACE and GRACE-FO accelerometer calibration parameters when using GOCO06s is also reported in Wöske et al. (2024). It appears that the averaged annual terms cause annual variations of the estimated biases. The GOCO06s gravity field model results in accelerometer biases that slightly deviate from the EIGEN-GRGS.RL04.MEAN-FIELD values to within 0.04 nm/s^2 for the X-axis and about 4.5 and 17 nm/s^2 for the Y- and Z-axes, respectively, within or close to the RMS-of-fit values of the linear regression.

When taking a close look at Fig. 3, an exponentially decaying trend can be observed during the early phase of the mission science operations for e.g. the time series of the Z-bias of accelerometer 5. Such trends can be identified for other accelerometers as well. When zooming in, a relatively strong exponentially decaying trend was observed for the X-axis bias of accelerometer 4, included at the bottom right of Fig. 4. Similar trends are observed for the GRACE accelerometers (Bettadpur 2009). Possible, but not conclusive causes are mentioned in Visser and Ijssel (2016), including possible aging of the instrument electronics or changing parasitic accelerations due to the gold wire that connects the accelerometer proof mass with the caging.

Compared to the results reported in Visser and Ijssel (2016), much lower RMS-of-fit values were obtained for the linear regressions (Figs. 3 and 4) for the ultra-sensitive accelerometer axes. For example, for the time series of common-mode acceleration biases, the RMS-of-fit is equal to about 0.29, 10.76, and 15.63 nm/s^2 for the X-, Y- and Z-axis, respectively, compared to 0.37, 16.44, and 48.64 nm/s^2 in Visser and Ijssel (2016). In addition, the one-dimensional (1D) RMS-of-fit of the kinematic PSO solutions improved from about 6.9 to about 2.6 cm, an improvement of $[1 - (\frac{2.6}{6.9})^2] \times 100 = 85\%$ in terms of variance. The same average 1D RMS-of-fit value of 2.6 cm was obtained for all individual accelerometers as well. The mean three-dimensional (3D) RMS-of-fit is 4.5 cm for the one-day kinematic orbits using EIGEN-GRGS.RL04.MEAN-FIELD and varies between 2.7 and 15.4 cm. Figure 5 displays the RMS-of-fit of the PSO-based common-mode accelerometer calibration as a function of time. It can be observed that the RMS-of-fit displays a growing trend with time. This is consistent with the increasing RMS of orbit differences between the PSO reduced-dynamic and kinematic solutions included in Fig. 5 as well and also reported in Arnold et al. (2023). The pattern can be explained by the reduced quality of the kinematic PSO solutions with growing levels of solar activity and associated ionospheric scintillations, which is also reflected by the percentage of missing kinematic PSO epochs, displayed in Fig. 5 as well.

For comparison, the 3D RMS of differences between the SLR-based two-day orbits and the PSO reduced-dynamic orbit solutions has a mean of 10.0 and varies between 5.0 and 27.6 cm. The two-day SLR fits have a mean of 2.8 cm with a minimum of 0.9 cm and a maximum of 6.6 cm. Compared to the results reported in Bruinsma et al. (2003), this shows the impressive improvements in the last two decades in terms of accelerometer instrument technology and in terms of force modeling.

Finally, it was mentioned in Sect. 3 that it is assumed that the center of the gradiometer coincides with the center-of-mass of the satellite. It has to be noted, however, that the center-of-mass of the satellite is drifting by about 3.7 cm along the flight axis during the period of science mode operations. For the SLR offset, this drift was taken into account (Table 1). It was found that shifting the center of the gradiometer by 3.7 cm along the X-axis results in a change of accelerometer bias of about 0.001, 0.1, and 0.5 nm/s^2 for the

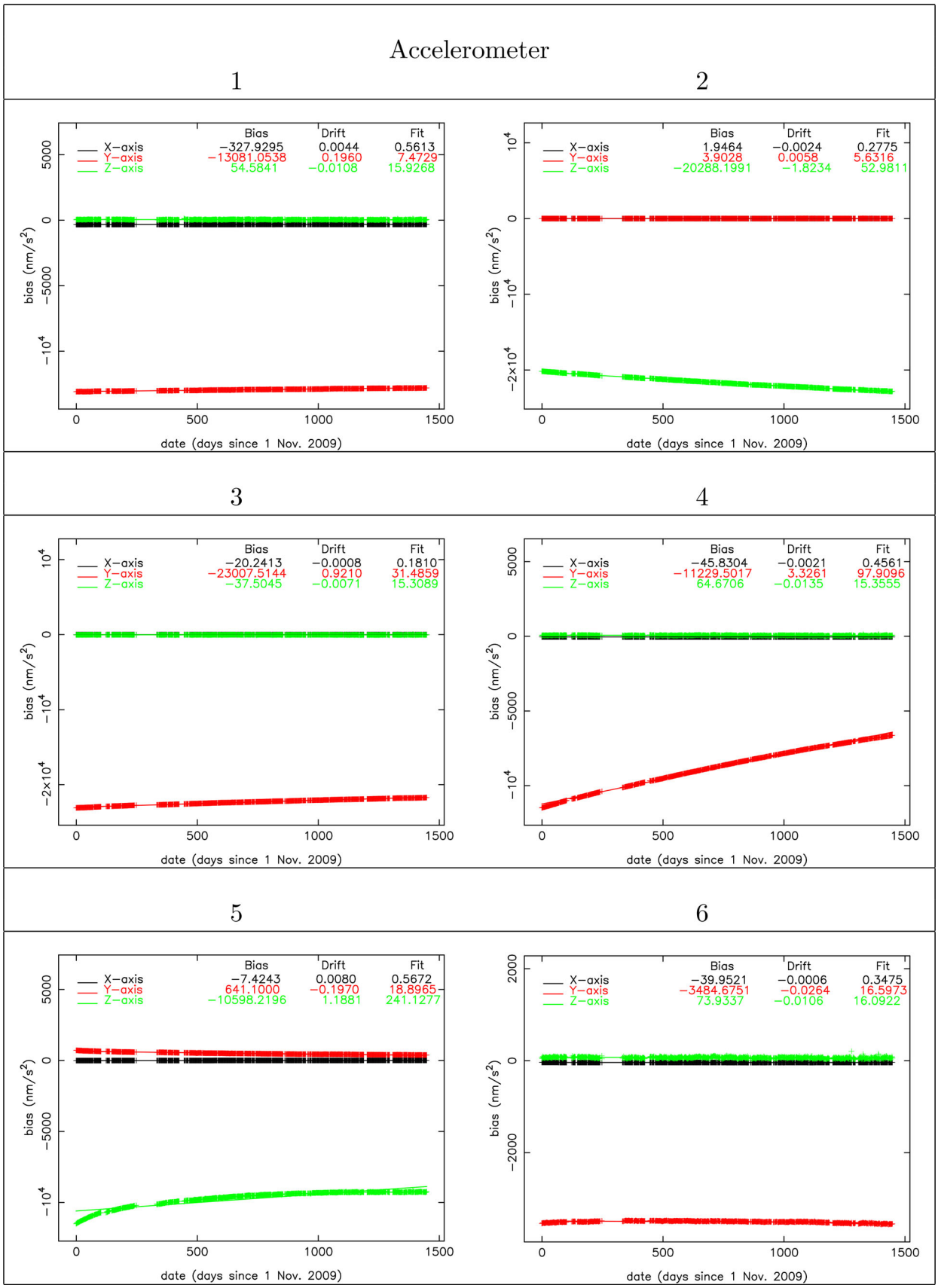

Fig. 3 Estimated accelerometer biases (nm/s^2) and drifts (nm/s^2/day) for the GOCE accelerometers 1 to 6 for the X-, Y- and Z-axes. Use was made of 1210 daily arcs with PSO kinematic orbit solutions as observables. The RMS-of-fit for a linear regression is displayed as well (nm/s^2), together with the bias (epoch 1 November 2009) and drift values of the linear regression

Table 2 Comparison between accelerometer bias and drift values obtained by precise orbit determination using the individual accelerometer observations, with the center-of-mass corrections applied, or common-mode (CM) accelerometer observations. The values obtained by SLR-based POD and using the GOCO06s model are included as well. The values hold for the linear regression with an epoch of 1 November 2009. Use was made of 1210 daily arcs with PSO kinematic orbit solutions as observables, except for the SLR-based solution where use was made of 51 2-day periods of SLR observations. The values in *italics* are relevant for the common-mode accelerometer observations and the values in **boldface** for the less sensitive axes. Finally, the RMS-of-fit values of the linear regression are also included

	Bias (nm/s^2)			Drift (nm/s^2/day)			Fit (nm/s^2)		
	X-axis	Y-axis	Z-axis	X-axis	Y-axis	Z-axis	X-axis	Y-axis	Z-axis
Acc. 1	*−327.9295*	**−13081.0538**	54.5841	*0.0044*	**0.1960**	−0.0108	*0.5613*	**7.4729**	15.9268
Acc. 2	1.9464	*3.9028*	**−20288.1991**	−0.0024	*0.0058*	**−1.8234**	0.2775	*5.6316*	**52.9811**
Acc. 3	−20.2413	**−23007.5144**	*−37.5045*	−0.0008	**0.9210**	*−0.0071*	0.1810	**31.4859**	*15.3089*
Acc. 4	*−45.8304*	**−11229.5017**	64.6706	*−0.0021*	**3.3261**	−0.0135	*0.4561*	**97.9096**	15.3555
Acc. 5	−7.4243	*641.1000*	**−10598.2196**	0.0080	*−0.1970*	**1.1881**	0.5672	*18.8965*	241.1277
Acc. 6	−39.9521	**−3484.6751**	*73.9337*	−0.0006	**−0.0264**	*−0.0106*	0.3475	**16.5973**	**16.0922**
CM	−186.8807	322.4901	19.4301	0.0012	−0.0956	−0.0092	0.2908	**10.7595**	*15.6252*
Average	−186.8800	322.5014	18.2146	0.0012	−0.0956	−0.0089			
SLR	−186.8700	339.2038	−30.4014	0.0010	−0.1227	−0.0080	0.2714	14.0698	96.4819
CM*	−186.8467	327.0613	2.4589	0.0011	−0.1061	0.0046	0.2886	13.1492	21.3582

* GOCO06s

X-, Y-, and Z-axis, respectively, which is much below the uncertainty level of the estimated biases.

4.2 Accelerometer scale factors

As outlined in Visser and Ijssel (2016), reliable accelerometer scale factors can be estimated by stacking the daily normal equations for the PSO-based accelerometer calibration. Similarly, it is expected this can be done for the two-day normal equations for the SLR observations. With this approach, one set of three accelerometer scale factors is estimated for the period of GOCE science mode operations. Thus, the scale factors will be based on 1210 daily arcs when using the kinematic PSO solutions and on 51 two-day orbital arcs when using SLR observations.

In Visser and Ijssel (2016), it was found that the scale factors are very close to one for the X- and Z-axes, but the scale factor deviates relatively much by 0.03 from one for the Y-axis. Use was made of the GOCO03s gravity field model (TUM 2025). For producing the GOCO03s model, the used GOCE data covers only the first 18 months of the science mode operations (November 2009 - April 2011). When using the EIGEN-GRGS.RL04.MEAN-FIELD or GOCO06s gravity field models, the deviation of about 0.03 for the Y-axis scale is reduced to about 0.002 and 0.007, respectively, when using the common-mode accelerometer observations (Table 3). For SLR, the common-mode scale factors are equal to 0.99986, 1.00434, 1.00162 for, respectively, the X-, Y- and Z-axis using 51 two-day arcs when using the EIGEN-GRGS.RL04.MEAN-FIELD gravity field model. Thus, very consistent accelerometer scale factors can be obtained by using SLR observations for the POD as well.

It is noted that both for the ultra-sensitive and less sensitive axes, the estimated scale factors are very close to one and no differences in performance can be observed. The quality of the estimated scale factors is driven by the ratio of the variance of the non-gravitational accelerations and the noise level of the accelerometer observations. For the less sensitive accelerometer axes, the noise level is in general orders of magnitude below the variance of the non-gravitational accelerations for the Y- and Z-axes, *cf.* Figure 2 in Visser and Ijssel (2016) which shows that this variance for a typical day, 15 November 2009, is about 100 nm/s^2 and about 30 nm/s^2, respectively. For most days, this variance is very low for the X-axis because of the DFC, e.g. only about 1.7 nm/s^2 for 15 November 2009. Continuous uninterrupted DFC would have made it impossible to estimate reliable accelerometer scale factors for the X-axis. However, there are several days for which orbit correction maneuvers are conducted with durations of several hours and with thrust levels from 200 to 1000 nm/s^2, which allows for a reliable estimation of accelerometer scale factors for the X-axes as well. With the uniform weight, i.e. meaning 1 m for the PSO kinematic position coordinates or SLR observations, this leads to formal $X/Y/Z$-axis scale factor errors of 0.0000079/0.0001710/0.0002368 and 0.0196289/0.0206502/0.0423002, respectively. Scaling these formal errors by the RMS-of-fit of the PSO kinematic position coordinates, 2.6 cm, or the SLR observations, 2.8 cm, leads to formal errors that are orders of magnitude below (PSO) or at the same order of magnitude (SLR) as the deviations from one reported in Table 3.

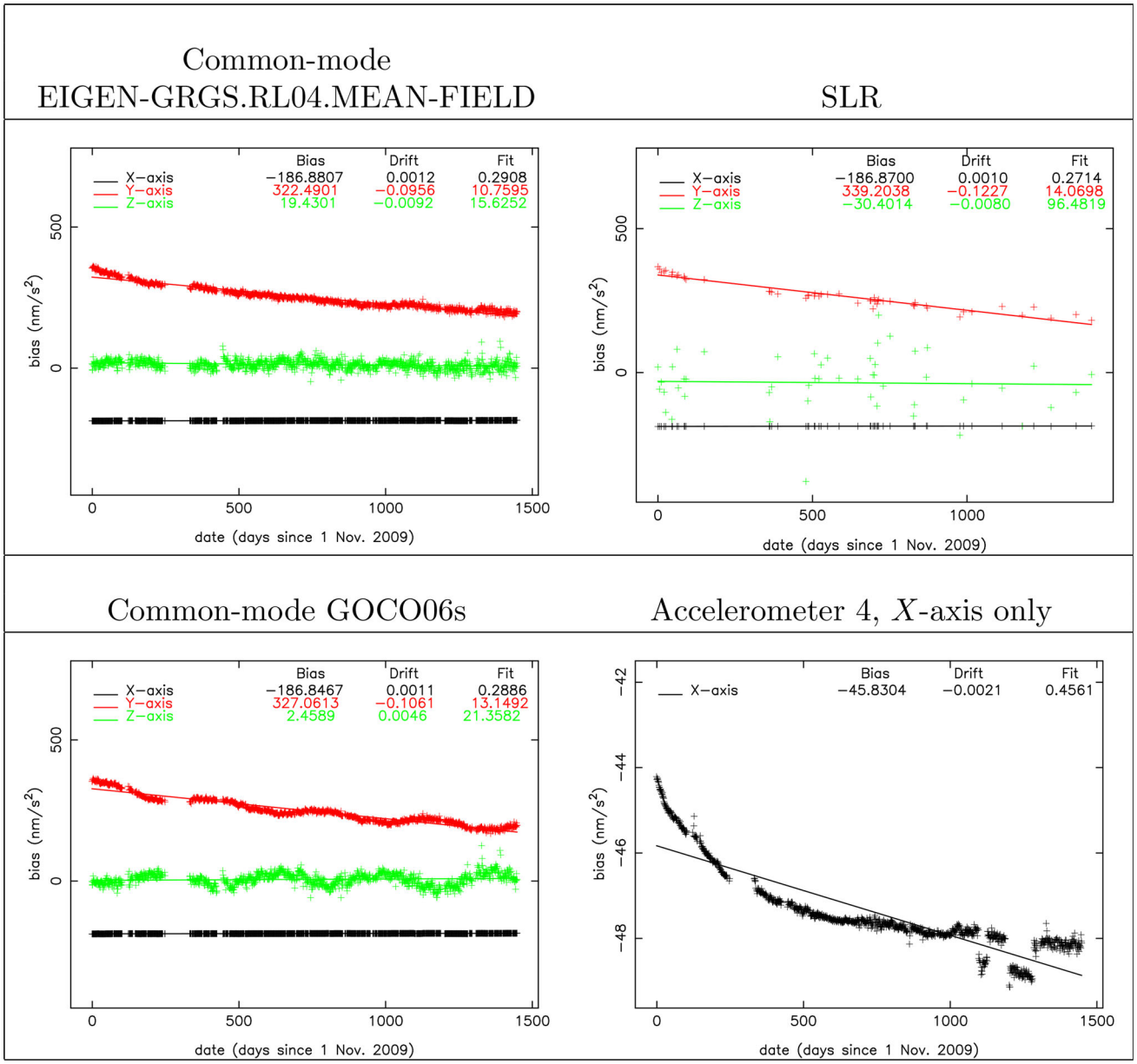

Fig. 4 Estimated accelerometer biases (nm/s^2) and drifts (nm/s^2/day) for the common-mode accelerometer observations for the X-, Y- and Z-axes. Use was made of 1210 daily arcs with PSO kinematic orbit solutions as observables. The biases estimated using 51 2-day periods of SLR observations or the GOCO06s model are included as well. The RMS-of-fit for a linear regression is also displayed (nm/s^2), together with the bias (epoch 1 November 2009) and drift values of the linear regression

5 Summary and conclusions

Several updates for the estimation of biases and scale factors of the GOCE individual accelerometers and common-mode accelerometer observations by POD were implemented. These updates include the use of the EIGEN-GRGS.RL04.MEAN-FIELD or GOCO06s gravity field models, the GOT 4.10 ocean tides model, updated de-aliasing products, and updated IERS standards. In addition to the kinematic PSO solutions as the basic observations in the POD, also SLR observations were used in a separate processing for estimating GOCE accelerometer calibration parameters.

Accelerometer biases were estimated for a total of 1210 days when using the kinematic PSO solution, and for 51 two-day arcs when using the SLR observations. As in Visser and Ijssel (2016), a high level of consistency was found for the bias values obtained for the individual accelerometers on the one hand and the bias values obtained for the common-mode accelerometer observations on the other hand. This was espe-

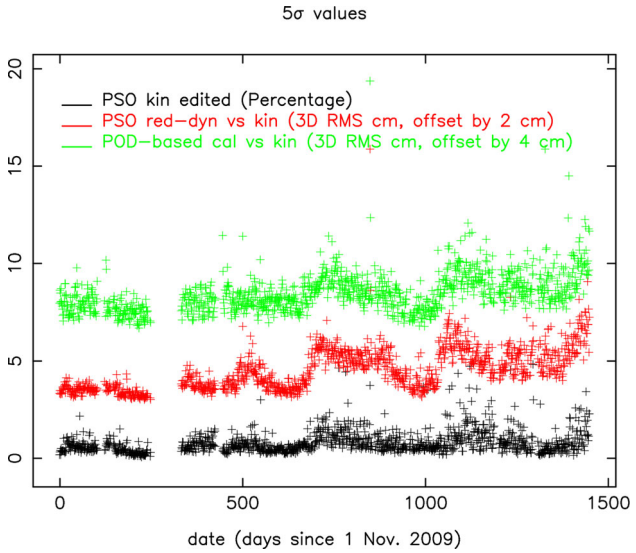

Fig. 5 3D RMS-of-fit of the kinematic PSO solutions (green), 3D RMS of orbit differences between the reduced-dynamic and kinematic PSO solutions (red), and the percentage of missing epochs in the kinematic PSO solution (black)

cially the case for the X-axis, predominantly pointing in the flight direction, for which the consistency is better than 0.001 nm/s^2 for the linear regression of the associated time series. Compared to the results reported in Visser and Ijssel (2016), an improvement from 6.9 cm to 2.6 cm or about 85% in terms of variance was obtained for the 1D RMS-of-fit of the kinematic PSO solutions. This RMS-of-fit is increasing toward the end of the mission, which can be attributed to a decreasing quality of the kinematic PSO solutions due to increased solar activity and, thus, higher ionospheric scintillations (Arnold et al. 2023).

One set of accelerometer scale factors for the period of GOCE science mode operations was obtained for which the deviations are much smaller than 0.005 for all axes when using the EIGEN-GRGS.RL04.MEAN-FIELD gravity field model. The 0.03 deviation for the Y-axis reported in Visser and Ijssel (2016) largely disappeared. The EIGEN-GRGS.RL04.MEAN-FIELD model included coefficients for the trend, annual and semi-annual gravity field changes with validity periods that cover the GOCE mission period of science mode operations. In addition, accelerometer bias values and scale factors were estimated with the GOCO06s model, which includes one set of trend and annual gravity field coefficients based on 15 years of data. The resulting time series of accelerometer bias values display annual variations, indicating that care has to be taken when using the annual terms of the GOCO06s model in precise orbit determinations.

In addition, it was found that the obtained bias and scale factor values could be verified by POD using SLR observations. Even with the sparse SLR tracking, the high-quality gravity field models and other updates allowed the compu-

Table 3 Scale factors estimated by dynamically fitting the PSO kinematic coordinates for the selected 1210 daily arcs. The values obtained with SLR observations for the common-mode accelerations are included as well (51 two-day arcs)

	SLR	CM	1	2	3	4	5	6
EIGEN-GRGS.RL04.MEAN-FIELD								
X-axis	0.99986	1.00013	1.00013	1.00009	1.00014	1.00014	1.00018	1.00012
Y-axis	1.00434	0.99782	0.99984	0.99712	0.99772	0.99716	0.99905	0.99962
Z-axis	1.00162	0.99403	0.99474	0.99469	0.99407	0.99276	0.99320	0.99335
GOCO06s								
X-axis	1.00047	1.00014	1.00013	1.00010	1.00014	1.00015	1.00019	1.00014
Y-axis	1.01200	1.00684	1.00882	1.00587	1.00738	1.00623	1.00835	1.00801
Z-axis	0.99990	1.00173	1.00254	1.00255	1.00160	1.00035	1.00074	1.00122

tation of dynamic orbit solutions with an average 3D RMS consistency of about 10 cm for two-day arcs, and for relatively well-tracked two-day arcs even as good as 5.0 cm. A high level of consistency was obtained for the bias values for the X- and Y-axes. The bias values for the Z-axis cannot be determined very precisely, but are consistent within the variation of the obtained values. The scale factors for the full mission are consistent at a level better than 0.001 for the X- and Z-axes, and better than 0.005 for the Y-axis.

Acknowledgements The European Space Agency is acknowledged for providing the GOCE observations. Part of the computations relied on the GEODYN software version 1911, which was kindly provided by the NASA Goddard Space Flight Center, Greenbelt, Maryland.

Author Contributions PV proposed the work, conducted the precise orbit determinations, analyzed the results and drafted the manuscript. JIJ supported the implementation of the used GEODYN 1911 software and reviewed the manuscript. CS helped analyzing the time series of obtained accelerometer calibration parameters and reviewed the manuscript.

Data Availability All GOCE observational data were taken from publicly available repositories (Sect. 2). This is also the case for the used force models (Sect. 3). The time series of estimated calibration parameters are available as an electronic supplement to this paper.

References

Arnold D, Grombein T, Schreiter L, Sterken V, Jäggi A (2023) Reprocessed precise science orbits and gravity field recovery for the entire GOCE mission. J Geod 97(67):1–22. https://doi.org/10.1007/s00190-023-01752-y

Altamimi Z, Rebischung P, Collilieux X et al (2023) ITRF2020: an augmented reference frame refining the modeling of nonlinear station motions. J Geod 97(47):1–22. https://doi.org/10.1007/s00190-023-01738-w

Bettadpur S (2009) Recommendation for a-priori Bias & Scale Parameters for Level-1B ACC Data (Version 2). GRACE TN-02, Version 2, 17 June 2009

Bruinsma S, Loyer S, Lemoine JM, Perosanz F, Tamagnam D (2003) The impact of accelerometry on CHAMP orbit determination. J Geod 77(1–2):86–93. https://doi.org/10.1007/s00190-002-0304-3

Balmino G, Rummel R, Visser P, Woodworth P, Johannessen J, Aguirre M (1999) Gravity field and steady-state ocean circulation explorer. Reports for mission selection, the four candidate earth explorer core missions, SP-1233 (1)

Cesare S, Catastini G (2005) Gradiometer on-orbit calibration procedure analysis. Technical Note to ESA, GO-TN-AI-0069, Issue 3, Alenia Aerospazio, May 2005

Chalmers (2025) Chalmers university website ocean loading calculator. https://barre.oso.chalmers.se/loading/l.php. last Accessed 25 Aug 2025

Dobslaw H, Bergmann-Wolf I, Poropat L, Dill R, Thomas M, Dahle C, Esselborn S, König R, Flechtner F (2017) A new high-resolution model of non-tidal atmosphere and ocean mass variability for de-aliasing of satellite gravity observations: AOD1B RL06. Geophys J Int 11(1):263–269. https://doi.org/10.1093/gji/ggx302

ESA (2025) GOCE on Earth online. European Space Agency, https://goce-ds.eo.esa.int/oads/access/collection/GOCE_Level_2, last Accessed 15 Sep 2025

Floberghagen R, Fehringer M, Lamarre D et al (2011) Mission design, operation and exploitation of the gravity field and steady-state ocean circulation explorer (GOCE) mission. J Geod 85(11):749–758. https://doi.org/10.1007/s00190-011-0498-3

Frommknecht B, Lamarre D, Meloni M, Bigazzi A, Floberghagen R (2011) GOCE level 1b data processing. J Geod 85(11):759–775. https://doi.org/10.1007/s00190-011-0497-4

GRACE (2018) GRACE_AOD1B_GRAV_GFZ_RL06. Ver. 6.0PO.DAAC, CA, USA. Dataset Accessed 16 Sep 2025. https://doi.org/10.5067/GRAOD-1BG06

Kvas A, Brockmann JM, Krauss S, Schubert T, Gruber T, Meyer U, Mayer-Gürr T, Schuh W-D, Jäggi A, Pail R (2021) GOCO06s–a satellite-onlyglobal gravity field model. Earth Syst Sci Data 13:99–118. https://doi.org/10.5194/essd-13-99-2021

Lyard FH, Allain DJ, Cancet M, Carrère L, Picot N (2021) FES2014 global ocean tide atlas: design and performance. Ocean Sci 17:615–649. https://doi.org/10.5194/os-17-615-2021

Lemoine J-M, Biancale R, Reinquin F, Bourgogne S, Gégout P (2019) CNES/GRGS RL04 Earth gravity field models, from GRACE and SLR data. GFZ Data Serv. https://doi.org/10.5880/ICGEM.2019.010

Mendes V, Prates G, Pavlis EC, Pavlis DE, Langley RB (2002) Improved mapping functions for atmospheric refraction correction in SLR. Geophys Res Lett 29(10):1–4. https://doi.org/10.1029/2001GL014394

NASA (2025) SGP: Space Geodesy Project. National Aeronautics and Space Administration, https://space-geodesy.nasa.gov/techniques/tools/GEODYN/GEODYN.html, last accessed 16 Sep 2025

Noll CE, Ricklefs R, Horvath J, Mueller H, Schwatke C, Torrence M (2019) Information resources supporting scientific research for the international laser ranging service. J Geod 93(11):2211–2225. https://doi.org/10.1007/s00190-018-1207-2

Nicholas JB, Rowlands DD, Luthcke SB, Yang HX, Loomis BD (2025) The GEODYN precision orbit determination software. ESS Open Archive. https://doi.org/10.22541/essoar.174051780.04684918/v1

Pail R, Bruinsma S, Migliaccio F, Förste C, Goiginger H, Schuh W-D, Höck E, Reguzzoni M, Brockmann JM, Abrikosov O, Veicherts M, Fecher T, Mayrhofer R, Krasbutter I, Sansò R, Tscherning CC (2011) First GOCE gravity field models derived by three different approaches. J Geod 85:819–843. https://doi.org/10.1007/s00190-011-0467-x

Petit G, Luzum B (2010) IERS Conventions 2010. International Earth Rotation and Reference Systems Service (IERS), IERS Technical Note No. 36

Pearlman MR, Noll CE, Pavlis EC (2019) The ILRS: approaching 20 years and planning for the future. J Geod 93:2161–2180. https://doi.org/10.1007/s00190-019-01241-1

Pavlis DE, Wimert J, McCarthy JJ (2015) GEODYN systems description. Technical report, Stinger Ghaffarian Technologies, Greenbelt Maryland

Ray RD (1999) A global ocean tide model from Topex/Poseidon altimetry: GOT99.2. Technical Report NASA Tech. Memo. 209478, Goddard Space Flight Center

Ray R (2013) Precise comparisons of bottom-pressure and altimetric ocean tides. J Geophys Res - Oceans 118:4570–4584. https://doi.org/10.1002/jgrc.20336

Siemes C, Borries C, Bruinsma S, Fernandez-Gomez I, Hładczuk N, IJssel J, Kodikara T, Vielberg K, Visser P (2023) New thermosphere neutral mass density and crosswind datasets from CHAMP, GRACE, and GRACE-FO. J Space Weather Space Clim 13:16

Siemes C, Rexer M, Schlicht A, Haagmans R (2019) GOCE gradiometer data calibration. J Geod 93:1603–1630. https://doi.org/10.1007/s00190-019-01271-9

Standish EM (1998) JPL planetary and lunar ephemerides, DE405/LE405. JPL IOM 312.F-98-048

TUM (2025) Gravity observation combination (GOCO). Technische Universität München, https://www.asg.ed.tum.de/iapg/forschung/schwerefeld/goco. last accessed 16 September 2025

Visser PNAM (2009) GOCE gradiometer: estimation of biases and scale factors of all six individual accelerometers by precise orbit determination. J Geod 83(1):69–85. https://doi.org/10.1007/s00190-008-0235-8

Visser PNAM, Ijssel JAA (2016) Calibration and validation of individual GOCE accelerometers by precise orbit determination. J Geod 90(1):1–13. https://doi.org/10.1007/s00190-015-0850-0

Wöske F, Huckfeldt M, Rievers B (2024) Tailored accelerometer calibration by POD for thermospheric density retrieval with GRACE and GRACE-FO. Adv Space Res 74(10):4517–4542. https://doi.org/10.1016/j.asr.2024.09.021